Conference Record of the

2003 IEEE Industry Applications Conference

38th IAS Annual Meeting

IAS 2003 Salt Lake City

Crossroads to Innovation

October 12-16

IAS IEEE INDUSTRY APPLICATIONS SOCIETY

IEEE

High-Frequency Electronic Ballast with Auto-Tracking Control for Metal Halide Lamps 1025
Chin S. Moo, Chunk K. Huang, Ying N. Hsiao, National Sun Yat-Sen University, R.O.C.

Operating Characteristics of Small-Wattage Metal Halide Lamps with Square Wave Current from 50 Hz to 50 kHz 1030
Ching R. Lee, Fortune Institute of Technology, R.O.C.;
Kuan H. Chen, Chin S. Moo, National Sun Yat-Sen University, R.O.C.

Sound Emissions From Pulse Operated High-Pressure-Sodium Lamps 1036
Walter Kaiser, Alexander Fernandez Correa, Ricardo Paulino Marques,
Escola Politécnica da Universidade de São Paulo, BRAZIL

A Study of the High Intensity Discharge Lamp-Electronic Ballast Interface 1043
Mark W. Fellows, Philips Lighting Company, USA

Deformation Analysis of Glass Vessel of High Pressure Mercury Lamp for LCD Projector 1049
Makoto Kai, Makoto Horiuchi, Tsuyoshi Ichibakase, Matsushita Electric Industrial Co., Ltd., JAPAN

Session 30—Wednesday, October 15th, 8:30 AM

POWER SYSTEMS ENGINEERING
Power Quality

Session Chair: Chris Melhorn, Electrotek Concepts, USA
Session Organizer: Matt Dozier, iDesign Systems, Inc., USA

Measurement and Characterization of DC Harmonics on the Taipei MRT System 1053
Ying-Tung Hsiao, Kuang-Chieh Lin, Tamkang University, TAIWAN

Explanation to Irregularities in the Dependence Between Voltage Sag Magnitude and the Tripping Level for Line Operated Synchronous Machines 1058
Fredrik Carlsson, KTH, SWEDEN

Operational Experience with a Nationwide Power Quality and Reliability Monitoring System 1063
William E. Brumsickle, Deepak M. Divan, Glen A. Luckjiff, John W. Freeborg, Roger L. Hayes,
SoftSwitching Technologies, USA

Mitigation of Voltage Dips Through Distributed Generation Systems 1068
K. J. P. Macken, R. J. M. Belmans, Katholieke Universiteit Leuven, BELGIUM;
M. H. J. Bollen, Chalmers University of Technology, SWEDEN

Steady-State and Dynamic Study of One-Cycle Controlled Three-Phase Active Power Filter 1075
Guozhu Chen, Zhejiang University, CHINA;
Keyue M. Smedley, University of California Irvine, USA

Session 31—Wednesday, October 15th, 8:30 AM

ELECTRIC MACHINES
Induction Machines II

Session Chair: Don Zinger, Northern Illinois University, USA
Session Organizer: Edward Lin, Baldor, USA

Modeling of Induction Machines Including Stator and Rotor Slot Effects 1082
Subhasis Nandi, University of Victoria, CANADA

Core Losses in Motor Laminations Exposed to High Frequency or Non-Sinusoidal Excitation 1090
Lotten T Mthombeni, P. Pillay, Clarkson University, USA

Measurement of Surge Propagation in Induction Machines 1098
T. Humiston, P. Pillay, Clarkson University, USA

Image Processing Method for the Visualization and Analysis of Iron Losses in Electrical Machines 1106
J. M. Reeve, C. Pollock, University of Leicester, UK

Development of the Two-Dimensional Oscillatory Actuator with the Attractive Force of Driving Source 1113
Susumu Torii, Hiroki Nakano, Toshihiro Yamaguchi, Daiki Ebihara, Musashi Institute of Technology, JAPAN;
Yuya Hasegawa, Katsuhiro Hirata, Matsushita Electric Works, Ltd., JAPAN

Apparent Impedance Angle Based Detection of Stator Winding Inter-turn Short Circuit Fault in Induction Motors 1118
Xu Boqiang, Li Heming, Sun Liling, North China Electric Power University CHINA

Design of Pole Change Single-Phase Induction Motor for Household Appliances 1126
H. Nam, S. K. Jung, G. H. Kang, J. P. Hong, Changwon National University, KOREA;
T. U. Jung, LG Electronics Inc., KOREA

Session 32—Wednesday, October 15th, 8:30 AM

INDUSTRIAL DRIVES
Speed Sensorless Controls

Session Chairs: Kambadkone Ashwin, National University of Singapore, SINGAPORE; Nicholas Nagel, MPC Products, USA
Session Organizer: Barbara Kenny, NASA Glenn Research Center, USA

Current Measurement Issues in Sensorless Control Algorithm using High Frequency Signal Injection Method 1134
Ji-Hoon Jang, Seung-Ki Sul, Seoul National University, KOREA;
Yo-Chan Son, Fairchild Semiconductor Korea, KOREA

Comparison of Saliency-based Sensorless Control Techniques for AC Machines 1142
Fernando Briz, Pablo García, University of Oviedo, SPAIN;
Michael W. Degner, Ford Motor Company, USA;
Robert D. Lorenz, University of Wisconsin–Madison, USA

Flux Observer Enhanced with Low-Frequency Signal Injection Allowing Sensorless Zero-Frequency Operation of Induction Motors 1150
Marko Hinkkanen, Veli-Matti Leppänen, Helsinki University of Technology, FINLAND;
Jorma Luomi, Helsinki University of Technology, FINLAND

Inverter Nonlinearity Effects in High Frequency Signal Injection-based, Sensorless Control Methods 1157
Juan M. Guerrero, Fernando Briz, University of Oviedo, SPAIN;
Michael Leetmaa, Robert D. Lorenzo, University of Wisconsin–Madison, USA;
Antonio Zamarrón, Technological Institute of León, MÉXICO

Acquisition of Rotor Anisotropy Signals in Sensorless Position Control Systems 1165
Joachim Holtz, University of Wuppertal, GERMANY;
Hangwen Pan, Panasonic Electronic Components, GERMANY

A Novel Method for Initial Rotor Position Estimation for IPM Synchronous Machine Drives 1173
Hyunbae Kim, Kum-Kang Huh, Robert D. Lorenzo, Thomas M. Jahns, University of Wisconsin–Madison, USA

A New Stable MRAS-based Speed and Stator Resistance Estimators for Sensorless Vector Control Induction Motor Drive at Low Speeds 1181
Mohamed Rashed, Fraser Stronach, Peter Vas, King's College, SCOTLAND

Session 33—Wednesday, October 15th, 8:30 AM

INDUSTRIAL POWER CONVERTER
Active Power Conditioners

Session Chair: J. Reichard, Integrated Electronics, USA
Session Organizer: G. Venkataramanan, University of Wisconsin–Madison, USA

Design and Implementation of a Direct-connected 11kV Power Conditioner 1189
Roger Brough, Shayne Crimp, Alister Gardiner, Industrial Research Ltd., NEW ZEALAND;
Hamish Laird, Simon Round, University of Canterbury, NEW ZEALAND

Comparisons in Circuit Configuration and Filtering Performance between Hybrid and Pure Shunt Active Filters 1195
Hirofumi Akagi, Sunt Srianthumrong, Yasuhiro Tamai, Tokyo Institute of Technology, JAPAN

Control Strategy for a Series Active Filter for the Neutral Conductor in a Building and Its Installation Point 1203
Keiji Wada, Shigenori Inoue, Tokyo Institute of Technology, JAPAN;
Toshihisa Shimizu, Tokyo Metropolitan University, JAPAN

Design of Pole Change Single-Phase Induction Motor for Household Appliances

H. Nam, S. K. Jung, G. H. Kang, and J. P. Hong
Dept. of Electrical Engineering
Changwon National University
Changwon, Gyeongnam, Korea, 641-773
haeggee@korea.com

T. U. Jung
Digital Appliance Company Research Lab.
LG Electronics Inc.
Changwon, Gyeongnam, Korea, 641-711
tujung@lge.com

Abstract—**This paper deals with the design of a pole change single-phase induction motor to reduce the harmonic components of the magnetic flux density in the air gap. The harmonics in the magnetic flux density distribution can have a significant detrimental effect on the characteristics of the machine such as crawling. In this paper, the magnetic flux density distribution is analyzed by analytical method and finite element method. Discrete Fourier Transform is used to analyze the harmonics and the characteristics are calculated from the equivalent circuit considering the harmonic components. The winding arrangement for the harmonic reduction is designed from the optimization method and the harmonic reduction of the improved models is verified through the experimental results.**

Keywords- pole change single-phase induction motor, harmonic components, magnetic flux density, distortion, crawling, Discrete Fourier Transform.

I. INTRODUCTION

Capacitor-run single-phase induction motors (SPIMs) are widely used in household appliances. The major reason is that the motors are fed directly from the commercial single-phase source without any control device [1]. A pole change SPIM in this paper is the capacitor-run SPIM that has two kinds of poles, 4-pole and 2-pole. Therefore, this motor is capable of variable speed operation and can expand the constant torque range using the pole change technique. In addition, it is maintenance-free and cheap in comparison with the motors such as 3-phase inverter motors and brushless DC motors, because it uses a pole change switch to change the speed without inverters or drives. Moreover, when the pole change SPIM, which can have two outputs and speeds at the same torque using the commercial frequency, is used for the compressor of household appliances, it can improve the system efficiency of the compressor even though the efficiency of the motor itself is a little low. Therefore, the household appliances using pole change SPIM is expected to be able to have more competitive power in cost and efficiency aspect than that using capacitor-run SPIMs and the inverter-type motors.

This paper deals with the design of the pole change SPIM. To improve the system efficiency of the compressor, the motor is designed focusing on high efficiency at 4-pole and the maximum torque at 2-pole. Moreover, pole change torque, which is torque when pole is changed, should be obtained.

The pole change SPIM is composed of a main winding, an auxiliary winding and a compensation winding. The main winding is used at both 4-pole and 2-pole. The auxiliary winding is used only for 4-pole, because it is started at 4-pole. When 4-pole is changed into 2-pole, the main winding is connected with the voltage source but the auxiliary winding is disconnected. At this time, the magnetic flux density distribution by only the main winding can result in severe distortion caused by harmonic components. The existence of harmonics is well known to have a significant detrimental effect on the characteristics of the machine such as crawling [2]. Therefore, to compensate both the magnetic flux density and the torque such as negative torque, the compensation winding is connected in parallel with the main winding at 2-pole operation. However, in spite of the compensation winding, speed-torque curves can be distorted by harmonic components, especially, the third and the fifth harmonics. Therefore, it is very important to calculate the accurate magnetic flux density and harmonics, and design the compensation winding for harmonic reduction.

In this paper, the magnetic flux density distribution in the air gap is analyzed by analytical method and Finite Element Method (FEM). Discrete Fourier Transformation (DFT) is used to analyze the harmonics in the magnetic flux density distribution. Using a prototype pole change SPIM, the characteristics are calculated from the equivalent circuit considering the harmonic components and the method is verified through the experimental results. Moreover, from the winding design using the optimization method to reduce the harmonic components, three models whose stators have 24 slots are designed and compared with the experimental results. Finally, the pole change SPIM, whose stator has 36 slots and the coil pitch is equal to the pole pitch, are presented.

II. POLE CHANGE TECHNIQUE

Fig. 1 shows the cross-section view of the pole change SPIM. The total slot number of the stator is 24, and two type windings are inserted in each slot. The symbols, M, A and C represent the main, the auxiliary and the compensation windings, respectively. The pole center at 2-pole is between slot number 6 and 7. Fig. 2 shows the winding patterns at 4-pole and 2-pole operations. When pole is changed from 4-pole to 2-pole, pole N′ and pole S′ of the main winding in Fig. 2(a) are changed into pole S″ and pole N″ in Fig 2(b), respectively. The auxiliary winding is disconnected and the compensation winding is connected in parallel with the main winding instead of the auxiliary winding as shown in Fig. 2(c).

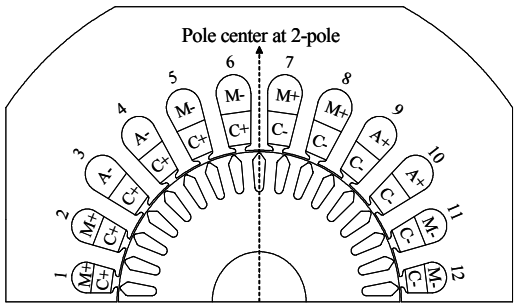

Figure 1. Cross-section of the pole change SPIM.

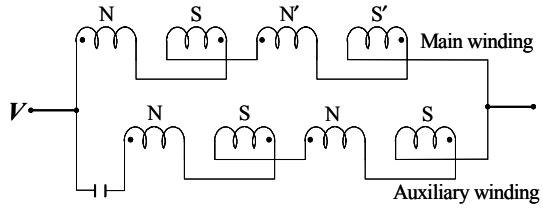

(a) Winding pattern at 4-pole operation.

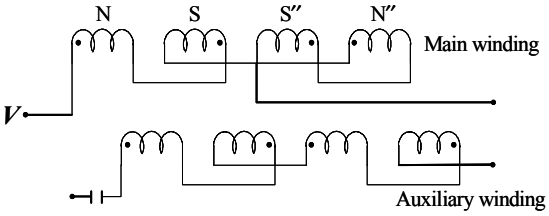

(b) Winding pattern by only the main winding at 2-pole operation.

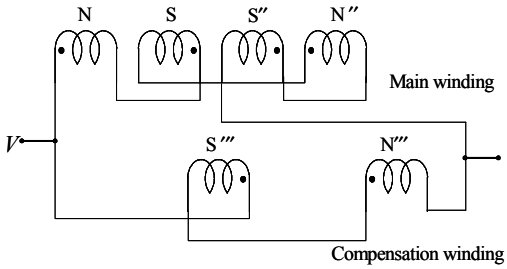

(c) Winding pattern by the main and the compensation windings at 2-pole operation.

Figure 2. Winding pattern according to the pole number.

Fig. 3 shows the magnetic flux density distribution by Finite Element Method (FEM), DFT of the magnetic flux density distribution and the speed-torque curves, which are obtained from the experimental results according to the existence of the compensation winding. In this paper, 90 deg. of rotor position in Fig. 3(a) corresponds to the pole center at 2-pole in Fig. 1. In Fig. 3(a) and (b), the unbalanced 6-pole of N-S-N-S-N-S occurs due to the harmonic components such as the third and the fifth order at 2-pole operation with only the main winding. As the results, the third harmonic component synchronizes the speed near 1,200 rpm, and the speed-torque curve is distorted and generates the negative torque, which is larger than the positive torque as shown in Fig. 3(c). Thus, the compensation winding is wound to compensate both the magnetic flux density distribution and torques such as the negative torque and the maximum torque at 2-pole.

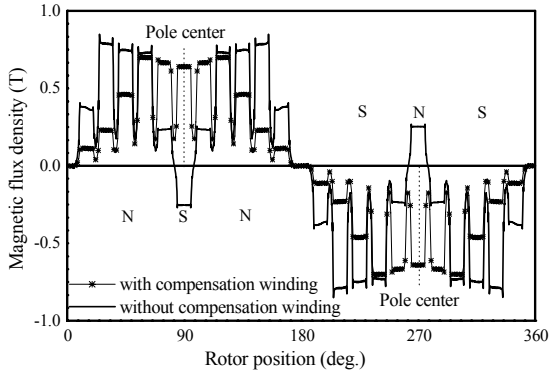

(a) Magnetic flux density distributions.

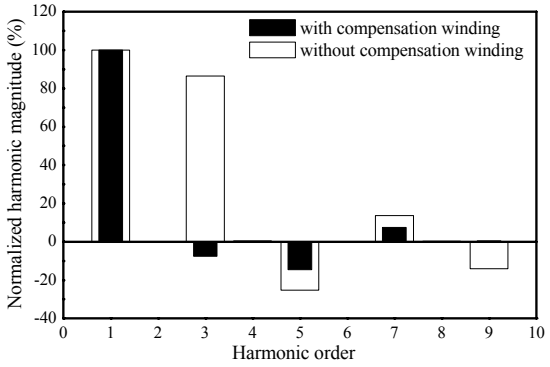

(b) DFT of the magnetic flux density distribution.

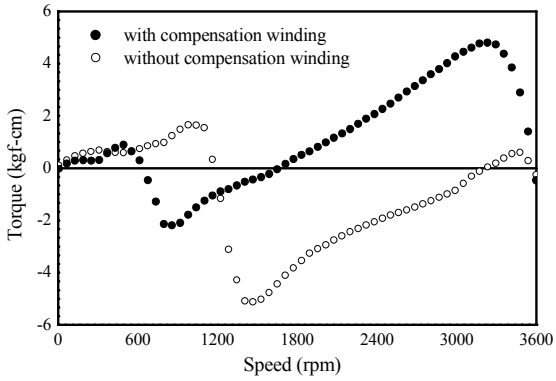

(c) Experimental results of the speed-torque curves.

Figure 3. Characteristics according to the compensation winding at 2-pole operation.

In Fig. 3, the magnetic flux density distribution of 6-pole is changed into that of 2-pole by the compensation winding, and the harmonic components as well as the negative torque are reduced. However, in spite of the compensation winding, the distortion of the speed-torque curve can be still produced. Therefore, it is very important to calculate the magnetic flux density distribution in the air gap and analyze the characteristics of the pole change SPIM considering the harmonic components.

III. ANALYSIS METHODS

A. Magnetic Flux Density Distribution in the Air Gap

The magnetic flux density distribution by analytical method is calculated as follows.

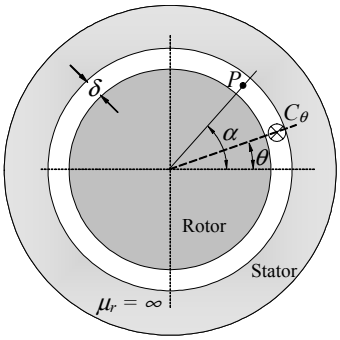

Figure 4. Illustration relating to the calculation of the field of conductors.

To avoid unnecessary mathematical complexity, certain simplifying assumption is made. The main simplifying condition is the assumption of the infinite relative permeability of iron ($\mu r=\infty$). It is assumed that the motor consists of two smooth coaxial cylinders made of a magnetic material and the cylinders are separated by the air gap in Fig. 4.

The magnetic flux density produced by an arbitrary system of conductors in the air gap is obtained by the superposition of the field densities of the individual conductors. The magnetic flux density $B(\alpha)$ of the individual turns at any point P having the coordinate α is obtained by using equation (1) [3].

$$B(\alpha) = \frac{\mu_0 C_\theta i}{\pi\delta} \sum_{n=1}^{\infty} \frac{1}{n} \sin n(\alpha - \theta) \tag{1}$$

where n is the harmonic order, C_θ is the number of conductors that are placed at the position θ and δ is the magnetic air gap.

B. Discrete Fourier Transform

DFT for the harmonic analysis of the magnetic flux density distribution can be expressed as equation (2).

$$a_n = \frac{2}{Num} \sum_{i=0}^{Num} b_i \sin\left(\frac{2\pi ni}{Num}\right) \tag{2}$$

where a_n is the n-th harmonic magnitude of the magnetic flux density, Num is the number of data and b_i is the magnetic flux density magnitude at each data. The ratio of the fundamental magnitude to the harmonic magnitude a_n/a_1 is used to obtain magnetizing reactance and secondary parameters of the n-th harmonic [4].

C. 4-Pole Characteristic Analysis

In order to analyze the characteristics of the capacitor-run SPIM by equivalent circuit, symmetrical-coordinate system considering unbalanced state is introduced as shown in Fig. 5.

Equation (3) and (4) are the positive and the negative voltages by the symmetrical-coordinate system, respectively.

$$\boldsymbol{V_P} = \left(\boldsymbol{V_M} - j\boldsymbol{V'_A}\right)/2 \tag{3}$$

$$\boldsymbol{V_N} = \left(\boldsymbol{V_M} + j\boldsymbol{V'_A}\right)/2 \tag{4}$$

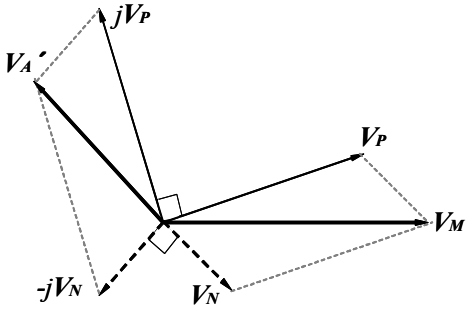

Figure 5. Symmetrical-coordinate system.

where V_P and V_N are the positive voltage and the negative voltage, respectively. The overall torque in equation (5) is calculated by the difference between the positive and the negative component torques and this equation expressed as the synchronous watt.

$$T = \frac{60}{2\pi N_0} (P_{2P} - P_{2N}) \tag{5}$$

where N_0 is the synchronous rotating velocity. P_{2P} and P_{2N} are the secondary output powers of the positive and the negative components, respectively, as shown in equation (6) and (7).

$$P_{2P} = \frac{R_2'}{s} \cdot \left|\boldsymbol{I_{2P}}\right|^2 \tag{6}$$

$$P_{2N} = \frac{R_2'}{2-s} \cdot \left|\boldsymbol{I_{2N}}\right|^2 \tag{7}$$

where I_{2P} and I_{2N} are the secondary input currents of the positive and the negative components, respectively.

D. 2-Pole Characteristic Analysis

The pole change SPIM at 4-pole operation is analyzed from the equivalent circuit by the symmetrical-coordinate system in order to consider the elliptical magnetic field. The main and the auxiliary windings are designed for 4-pole and there are few harmonics in the magnetic flux density distributions. Thus, the equivalent circuit is composed of the fundamental component. On the other hand, the main winding for 4-pole operation is also used at 2-pole operation. Therefore, the magnetic flux density distribution with only the main winding can become severely distorted by the harmonic components.

Fig. 6, as suggested by Alger and others, shows the equivalent circuit considering the harmonic components for the characteristic analysis at 2-pole operation [5]. It is a useful concept to visualize the electromagnetic behavior of the various space harmonic as being similar to the behavior of separate motors, with a common stator winding and a common shaft, but with magnetizing reactances and secondary impedances corresponding respectively to the air gap flux wave of each specific harmonic. Therefore, the effect of the various harmonic torques on the fundamental speed-torque

curves can be evaluated from the equivalent circuit. The phase quantities V_1, R_1, R_2, X_2 and X_M of the circuit are identical to those of the standard equivalent circuit, such as that shown in Fig.6. The magnetizing reactance of each of the harmonics, such as $X_{M\text{-}5}$, is based on the component of air gap flux of that particular harmonic. In addition, the slip function of $R_{2\text{-}n}$ for each harmonic is set up for the rotor slip for that particular harmonic and is dependent on the order of the harmonic and on whether the harmonic field is positive (or forward) rotating or negative (or backward) rotating.

Thus, the n-th slip function can be expressed as equation (8) if it is a forward rotating field and it can be expressed as equation (9) if it is a backward rotating field [5].

$$s_{pn} = 1 - n(1-s) \tag{8}$$

$$s_{nn} = 1 + n(1-s) \tag{9}$$

where n is the order of the harmonic, s is the slip of the fundamental component. Considering the fundamental component as a harmonic of the first order, the harmonic order of the pole change SPIM consists of odd terms only.

Fig. 7 shows the flow chart for the characteristic analysis at 2-pole operation. The phases of the main and the compensation windings are same. Therefore, the mutual effect on the two windings should be considered. Moreover, the characteristics of each winding are calculated by using the equivalent circuit of Fig. (6), respectively. The total torque can be obtained from superposition of the torques by the main and the compensation windings according to slip.

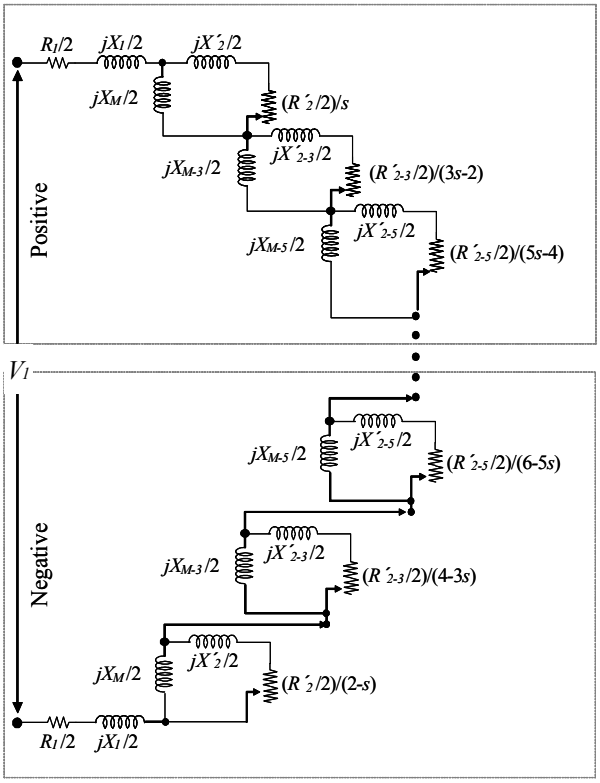

Figure 6. Equivalent circuit considering the harmonic components.

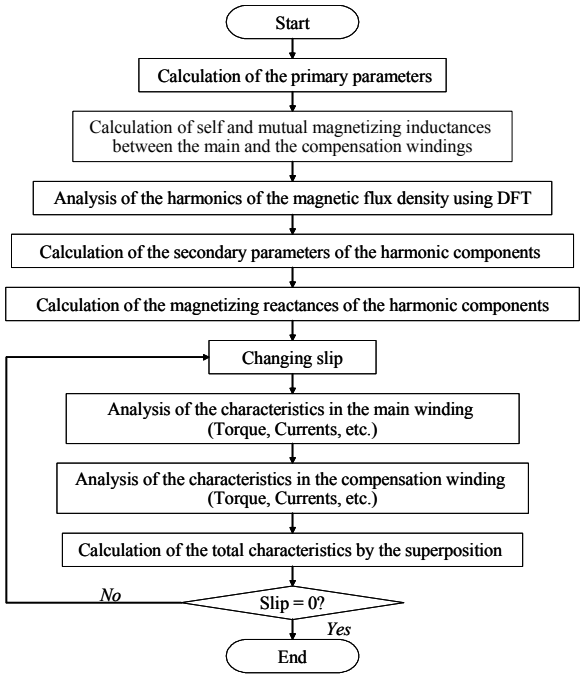

Figure 7. Flow chart for the characteristic analysis at 2-pole operation.

TABLE I
BRIEF SPECIFICATIONS OF ANALYSIS MODEL

Item	Value	Unit
Input voltage	220	V
Frequency	60	Hz
No. of slots (stator/rotor)	24/34	
Air gap length	0.3	mm
Stack length	48.0	mm
Outer diameter of rotor	60.0	mm
Rated torque	4.4	kgf-cm
Output power (2-/4-pole)	160/80	W

E. Characteristic Analysis Results

To verify the presented analysis method in this paper, the characteristics are analyzed using the prototype model that has the specifications of the pole change SPIM as shown in Table I. Input voltage is 220 V and frequency is 60 Hz. While output power and synchronous speed are 160 W and 3,600 rpm at 2-pole operation, those of 4-pole operation are 80 W and 1,800 rpm, respectively.

Fig. 8(a) shows the magnetic flux density distribution in the air gap using the analytical method in comparison with the FEM. The effect on the saturation can be considered by the FEM, but not by the analytical method. Therefore, the difference between the harmonic analysis results by two methods occurs as shown in Table. 2. As the results, the speed–torque curve of the analysis model by the experimental result is affected by the fifth order harmonic component , while that of the analysis model by the simulation result is more affected by the third order harmonic component than the fifth order harmonic component as shown in Fig 8(c).

Even though the speed-torque curve of the analysis result differs from that of the experimental result, the analysis results by the presented analytical method show the effect of the

harmonics and the important torques such as the pole change torque and the maximum torque at 2-pole can be estimated. Thus, this presented method is used for the characteristic analysis and the winding design to reduce the harmonic components of the pole change SPIM in this paper.

TABLE II
HARMONIC ANALYSIS RESULTS

Harmonic order	Analytical method (%)	FEM (%)
1	100.0	100.0
3	-17.6	-7.5
5	-7.3	-14.5
7	4.0	7.5

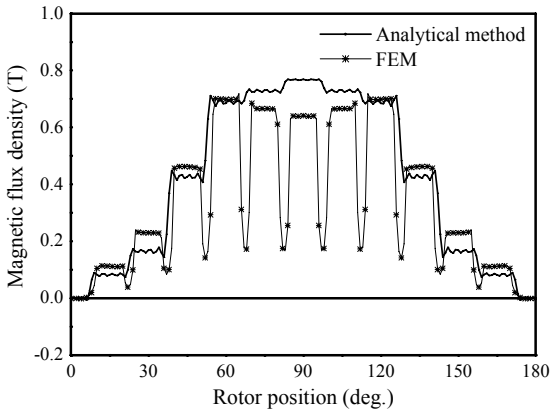

(a) Magnetic flux density distribution at 2-pole.

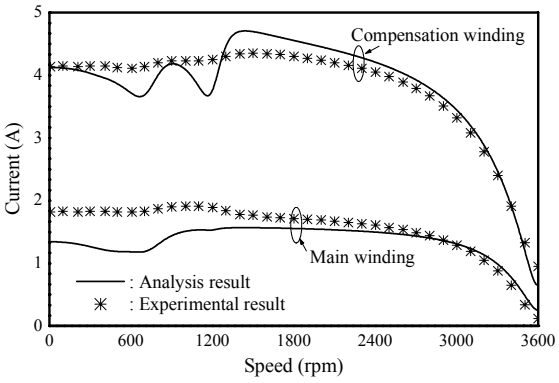

(b) Speed-current curves at 2-pole operation.

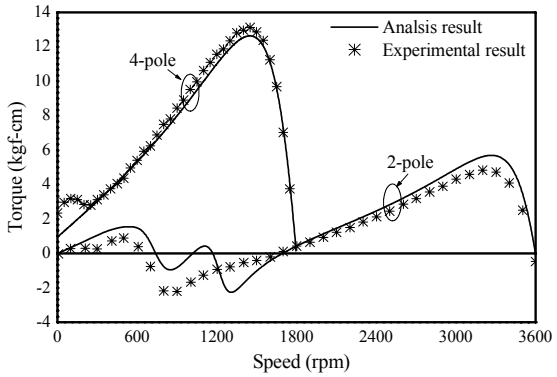

(c) Speed-torque curves.

Figure 8. Characteristic analysis results of the prototype model.

IV. DESIGN FOR HARMONIC REDUCTION

A. Procedure of Winding Design

In Fig. 8, in spite of the compensation winding, the speed-torque curve is distorted by the third and the fifth harmonic components. Therefore, it is very important to design the compensation winding for harmonic reduction. Fig. 9 shows the flow chart of the winding design. The magnetic flux density and the harmonic analysis are calculated by the analytical method. In the figure, I_m and I_c are the currents of the main and the compensation windings, respectively. Distortion factor *FN*, the ratio of the fundamental component to the average harmonics, represents the distortion effect by the harmonics and can be expressed as equation (10).

$$FN = \frac{\sqrt{\sum_{i=1,3,5} V_i^2}}{V_1} \tag{10}$$

where, V_1 and V_i are the magnitude of the fundamental magneto-motive force(MMF) and the harmonic MMF, respectively. The number of turns is determined from optimization using conjugated (CG) method. From the determined compensation winding, the performances of the pole change SPIM are analyzed by the equivalent circuit considering the harmonics as shown in Fig. 6 [5].

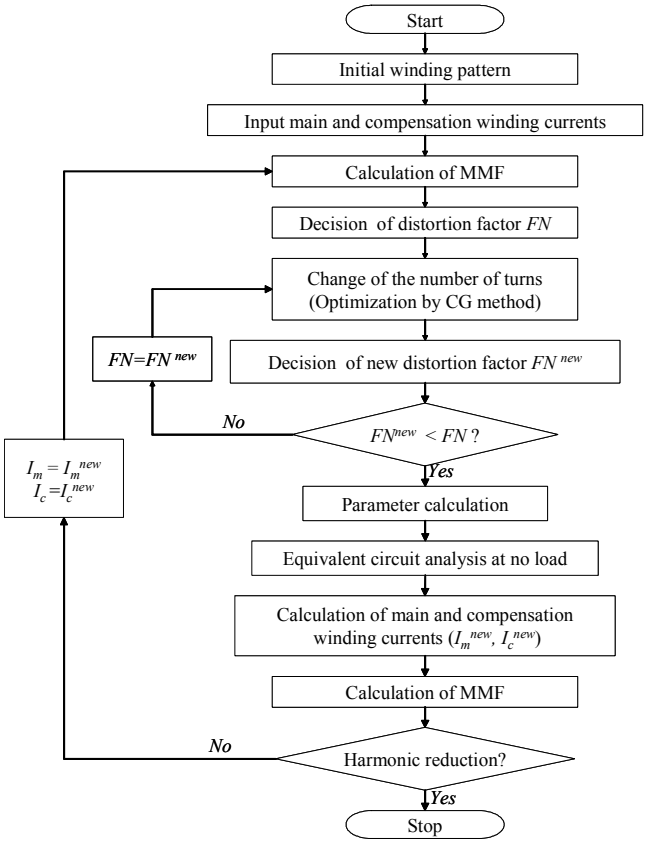

Figure 9. Flow chart for the winding design.

B. Characteristics according to Coil Pitch

Fig. 10 shows the winding distributions according to coil pitch of the main winding. In Fig. 10(a), the coil pitch of the main winding is less than the pole pitch. The winding distribution by only the main winding without the compensation winding induces opposite pole near 90 deg. of rotor position as shown in Fig. 3(a). Therefore, to compensate the magnetic flux density distributions using the compensation winding for the harmonic reduction, this type motor needs many turns in the slots near 90 deg. of rotor position. On the other hand, Fig. 10(b) and Fig. 11 show the winding distribution and the magnetic flux density distribution when the coil pitch of the main winding is equal to the pole pitch. This winding distribution induces the same pole in part A, that is, 90deg. of rotor position. Therefore, the slot area as well as the number of turns in part A can be reduced.

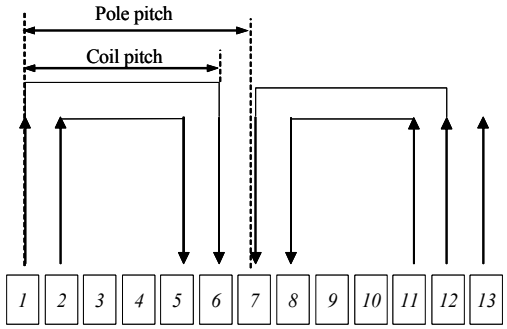

(a) Short pitch.

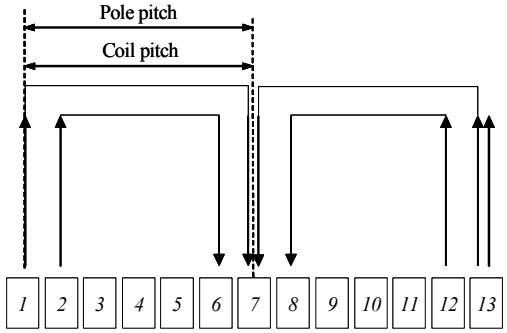

(b) Full pitch.

Figure 10. Winding distributions according to coil pitch of the main winding.

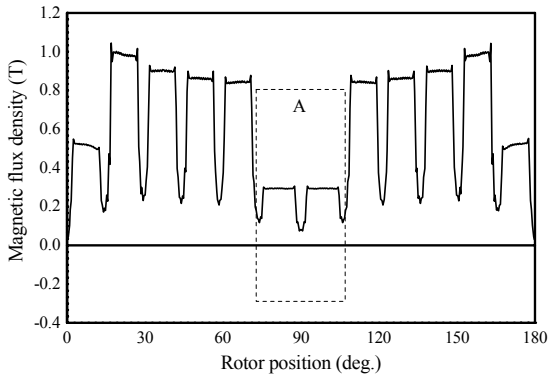

Figure 11. Magnetic flux density distribution by only the main winding at 2-pole.

C. Improved Models

The four pole change SPIMs are designed to reduce the harmonic components of the magnetic flux density distribution in the air gap and the specifications of the improved models are represented in Table III. In Model I and II, rated output powers of 2-pole and 4pole are 160 W and 80 W, respectively. Model III has rated output powers of 115 W at 2-pole and 55 W at 4-pole. The number of stator and rotor slots and the rotor volume in the models are same. The three models, which have shot pitch winding distribution, are manufactured and have both the analysis and the experimental results.

In Model IV, rated output powers of 2-pole and 4pole are 160 W and 80 W, respectively, and equal to those of model I and II. But, the winding distribution, the numbers of stator and rotor slots and the rotor volume are different. Model IV has the only analysis results, because it is not manufactured.

While model I and II have the PTC resistance, which is connected in parallel with the running capacitance and the same torque per rotor volume, model III and IV substitute the starting capacitance and the switch for the PTC resistance and have the same torque per rotor volume.

Fig. 12 shows the test apparatus for the pole change SPIMs.

D. Analysis and Experimental Results

Fig. 13 shows the MMF distributions in the air gap according to rotor position of the four models at 2-pole by the main and the compensation windings.

The harmonic analysis results of the models are shown in table IV. The magnitudes according to harmonic order are lower than 5.0 %. Especially, those of model IV are less than 0.5 %.

Fig. 14 shows the speed-torque curves of the four models. This results show that the harmonic effect such as crawling is reduced in comparison with the prototype model. As shown in Fig. 14(d), the speed-torque curve at 2-pole in the model IV is affected little by the harmonic components.

TABLE III
BRIEF SPECIFICATIONS OF IMPROVED MODELS

Item		Model I	Model II	Model III	Model IV
Rated output power of 2-/4-pole(W)		160/80	160/80	115/55	160/80
Rated torque (kgf-cm)		4.4	4.4	3.1	4.4
No. of slots (stator/rotor)		24/34	24/34	24/34	36/44
Rotor volume (×10e+3mm2)		135.7	135.7	135.7	192.9
Torque per rotor volume (×10e-6kgf-cm/mm2)		32.4	32.4	22.8	22.8
No. of series turns	Main winding	1120	1280	1424	1264
	Auxiliary winding	560	1080	1184	1240
	Compensation winding	800	792	756	764
PTC resistance (Ω)		33	33	-	-
Starting capacitance (μF)		-	-	8	12
Running capacitance (μF)		5	3	2	3

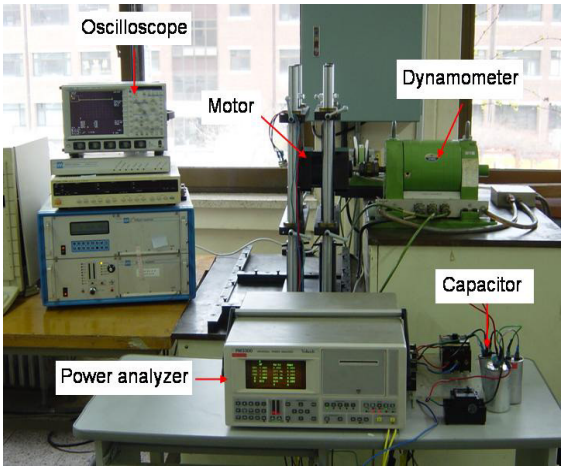

Figure 12. Test apparatus.

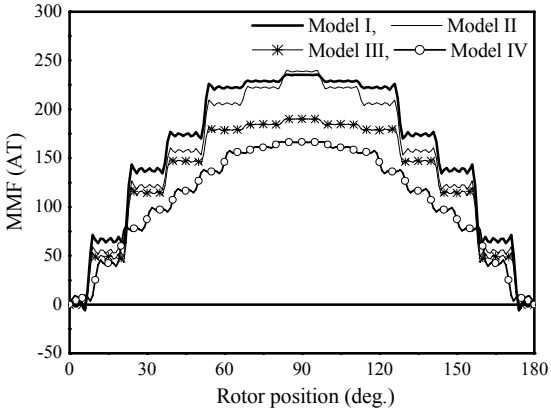

Figure 13. MMF distributions in the air gap of the models.

TABLE IV
HARMONIC ANALYSIS RESULTS

Harmonic order	Model I	Model II	Model III	Model IV
1	100.0	100.0	100.0	100.0
3	3.4	3.9	4.3	0.26
5	0.9	0.0	2.0	0.0
7	0.6	0.4	1.0	0.15

Table V shows the experimental results at the rated output power except for model IV. The values of the model IV are the analysis results. While the model I is focused on maximum torque at 2-pole and pole change torque, the model II is focused on efficiency at 4-pole. Therefore, the maximum torque at 2-pole and the pole change torque of the model I are 16.67 kgf-cm, and 6.00 kgf-cm, respectively, and larger than 13.00 kgf-cm, and 4.00 kgf-cm of the model II. On the other hand, the efficiency at 4-pole of the model II is 75.32 % and higher than 69.64 % of the model I.

The model III, which differs from the model I and II in the rated output power, is designed to improve torque such as the maximum torque at 2-pole and the pole change torque for 3.14 kgf-cm of the rated torque, and the efficiency at 4-pole. Therefore, the maximum torque at 2-pole is 14.40 kgf-cm, 4.65 times of the rated torque, pole change torque is 5.24 kgf-cm, 1.69 times of the rated torque, and the efficiency at 4-pole is 74.40 %.

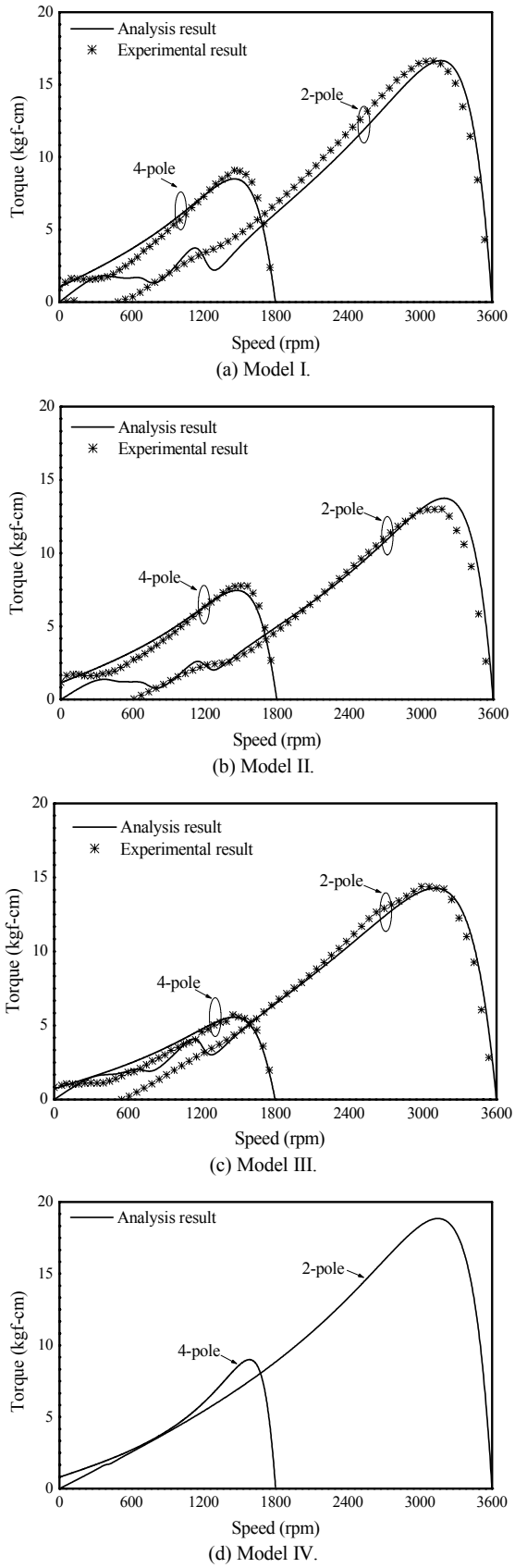

Figure 14. Speed-torque curves according to models at 2-pole and 4-pole.

TABLE V
EXPERIMENTAL RESULTS AT RATED OUTPUT POWER

Item		Model I	Model II	Model III	Model IV
4-pole	Rated output (W)	79.45	79.49	55.40	79.26
	Rated torque (kgf-cm)	4.49	4.52	3.14	4.41
	Maximum torque (kgf-cm)	9.09	7.50	5.53	9.00
	Line current (A)	0.57	0.52	0.40	0.43
	Main current (A)	0.75	0.52	0.44	0.36
	Aux. current (A)	0.49	0.36	0.23	0.46
	Efficiency (%)	69.64	75.32	74.40	81.20
2-pole	Rated output (W)	162.0	157.86	115.00	160.02
	Rated torque (kgf-cm)	4.38	4.38	3.10	4.38
	Maximum torque (kgf-cm)	16.67	13.00	14.40	18.85
	Line current (A)	2.04	1.76	1.35	1.58
	Main current (A)	0.66	0.41	0.10	0.41
	Comp. current (A)	1.38	1.35	1.25	1.17
Starting torque (kgf-cm)		5.52	7.29	5.53	2.09
Pole change torque (kgf-cm)		6.00	4.00	5.24	8.06

V. CONCLUSION

This paper deals with the analysis method by the equivalent circuit considering harmonic components and the winding design to reduce the harmonics of the pole change SPIM. From the analysis and the experimental results of the prototype pole change SPIM, the distortion of speed-torque curves by the harmonics is shown.

The four improved models for the reduction of the harmonics are designed. The three models, the model I, II and III, are manufactured and tested. From the experimental results, these models are verified that the harmonic components are reduced and the maximum torque at 2-pole and the pole change torque are obtained. In addition, the efficiency at 4-pole in the model III is improved.

Even though the model IV is not fabricated, the analysis results show the fact that the harmonic components and the number of turns of the compensation winding near 90deg. of rotor position are more reduced, and the pole change torque, the maximum torque at 2-pole, and the efficiency at 4-pole are more improved when the coil pitch is equal to the pole pitch.

REFERENCES

[1] H. Nam, K. H. Ha, J. J. Lee, J. P. Hong, and G. H. Kang, "A study on iron loss analysis method considering the harmonics of the flux density waveform using iron loss curves tested on Epstein samples," *IEEE Trans. Magn.,* vol. 39, no. 3, pp. 1472-1475, May 2003.

[2] H.A. Toliyat, and N. Sargolzaei, "A Comprehensive Method for Transient Modeling of Single Phase Induction Motors Including the Space Harmonics," *Journal of Electric Machines and Power Systems,* vol. 26, no. 3, pp. 221-234, 1998.

[3] B. Heller and V. Hamata, *Harmonic Field Effects in Induction Machine*. Elsevier Scientific Publishing Company, 1977.

[4] C. G. Veinott, Theory and Design of Small Induction Motors. McGRAW HILL, 1959.

[5] P. L. Cochran, Polyphase Induction Motors, Analysis, Design, and Application. Marcel dekker, 1989.